Remote sensing inversion and spatial variation of land surface temperature over mining areas of Jixi, Heilongjiang, China

Jia-shuo Cao[1,2], Zheng-yu Deng[1,2], Wen Li[1] and Yuan-dong Hu[1,2]

[1] College of Landscape Architecture, Northeast Forestry University, Harbin, Heilongjiang, China
[2] Key Laboratory for Garden Plant Germplasm Development & Landscape Eco-Restoration in Cold Regions of Heilongjiang Province, Harbin, Heilongjiang, China

ABSTRACT

Background. Jixi is a typical mining city in China that has undergone dramatic changes in its land-use pattern of mining areas over the development of its coal resources. The impacts of coal mining activities have greatly affected the regional land surface temperature and ecological system.

Methods. The Landsat 8 Operational Land Imager (OLI) data from 2015 and 2019 were used from the Jiguan, Didao, and Chengzihe District of Jixi in Heilongjiang, China as the study area. The calculations to determine the land-use classification, vegetation coverage, and land surface temperature (LST) were performed using ArcGIS10.5 and ENVI 5.3 software packages. A correlation analysis revealed the impact of land-use type, vegetation coverage, and coal mining activities on LSTs.

Results. The results show significant spatial differentiation in the LSTs of Jixi City. The LSTs for various land-use types were ranked from high to low as follows: mining land > construction land > grassland > cultivated land > forest land > water area. The LST was lower in areas with high vegetation coverage than in other areas. For every 0.1 increase in vegetation coverage, the LST is expected to drop by approximately 0.75 °C. An analysis of mining land patches indicates that the patch area of mining lands has a significant positive correlation with both the average and maximum patch temperatures. The average patch temperature shows a logarithmic increase with the growth of the patch area, and within 200,000 m^2, the average patch temperature increases significantly. The maximum patch temperature shows a linear increase with the patch area growth, and for every 100,000 m^2 increase in the patch area of mining lands, the maximum patch temperature increases by approximately 0.81 °C. The higher the average patch temperature of mining land, the higher the temperature in its buffer zone, and the greater its influence scope. This study provides a useful reference for exploring the warming effects caused by coal mining activities and the definition of its influence scope.

Subjects Coupled Natural and Human Systems, Environmental Contamination and Remediation, Environmental Impacts, Spatial and Geographic Information Science
Keywords Jixi, Mining areas, Land surface temperature, Spatial variation, Coal mining activities, Land-use types, Vegetation coverage

Submitted 20 April 2020
Accepted 6 October 2020
Published 25 November 2020

Corresponding author
Wen Li, liwen@nefu.edu.cn

Academic editor
Todd Anderson

Additional Information and Declarations can be found on page 20

DOI **10.7717/peerj.10257**

How to cite this article Cao J-S, Deng Z-Y, Li W, Hu Y-D. 2020. Remote sensing inversion and spatial variation of land surface temperature over mining areas of Jixi, Heilongjiang, China. *PeerJ* **8**:e10257 http://doi.org/10.7717/peerj.10257

INTRODUCTION

The land surface temperature (LST) comprehensively reflects the energy exchange between land and the atmosphere, which is an important geophysical parameter in the ground-air system (*Li et al., 2016*; *Zhu et al., 2016*). Coupling the inversion results of LST with other parameters, such as land-use type and vegetation coverage, provides a scientific basis for ecological environmental protection (*Li et al., 2014*; *Liang & Zhai, 2014*; *Xu, He & Huang, 2013*; *Zhang et al., 2013a*; *Zhang et al., 2013b*). The commonly used LST inversion algorithms are divided primarily into the single-channel algorithm, multi-channel algorithm, and split-window algorithm (*Zhu et al., 2016*). Among them, the single-channel algorithms include the atmospheric correction method, Mono-window algorithm, and the Jiménez-Muñoz J.C single-channel algorithm (*Qin, Karnieli & Berliner, 2001*; *Jiménez-Muñoz et al., 2008*). The multi-channel algorithms mainly include the day-night method, temperature emissivity separation algorithm, and graybody emissivity method (*Gan et al., 2006*; *Gillespie et al., 2002*; *Zhang et al., 2000*). The split window algorithm is based mostly on data from the Landsat-TIRS, NOAA-AVHRR, and TERRA-MODIS (*Rozenstein et al., 2014*; *Qin & Karnieli, 2001*; *Mao et al., 2005*).

Due to aggravation of the heat island effect, current research on LSTs is mostly focused on urban areas. Analyzing differences in LSTs for different land-use types optimizes the distribution of green space from the perspective of landscape patterning to reduce the heat island effect (*Liu, 2016*). However, mining areas, which are often affected by high temperatures and cause safety problems, have not attracted sufficient attention and are rarely studied.

Some research has shown that in the resource development process for resource-based cities, the land-use patterns in mining areas are constantly changing, which causes a series of impacts on the regional ecological environment (*Li et al., 2018*; *Chabukdhara & Singh, 2016*; *Xie, Wang & Fu, 2011*). Therefore, research focusing on coupling between land-use patterns in mining areas and the ecological environment indicators, such as the LST, water environment quality, and biodiversity, has become vital to environmental sustainability (*Zhou & Wang, 2014*; *Xiao, Hu & Fu, 2014*; *Hu, Duo & Wang, 2018*; *Bian et al., 2018*). Current research on land surface temperatures in mining areas mainly includes the temporal and spatial distribution characteristics of the surface temperature, the impact of ecological disturbance on the surface temperature, and others, where the scales are mostly at macro-regions (*Li, Yang & Lei, 2017*; *Qiu & Hou, 2013*; *Xie, Wang & Fu, 2011*). This study specifically analyzes the overall and local distribution characteristics of LSTs from smaller scales to explore the radius of influence of high-temperature points. This provides a reference to establish heat alerts in mining areas.

Jixi is a typical mining city in China that has undergone dramatic changes in its land-use pattern in the mining area during the development of coal resources. Significant amounts of cultivated land, forest land, and other land types have been replaced by industrial and mining sites, which has greatly affected the regional ecological environment. Impacts such as the atmospheric diffusion of pollutants and the rise of LSTs have affected the regional landscape and ecological systems (*Pan et al., 2013*; *Liao, 2009*). This paper uses data from

the Landsat 8 OLI remote sensing images from 2015 and 2019 to determine LSTs using the radiation conduction equation over the study area, which encompasses the Jiguan, Didao, and Chengzihe District of Jixi. We analyzed the spatial differentiation and correlations of the LST with the land-use type and vegetation coverage to provide a theoretical framework to reduce the heat island effects caused by local urban development and coal mining activities.

MATERIALS & METHODS

Overview of the study area

The study area encompasses the Jiguan, Didao, and Chengzihe District of Jixi, which are the main mining lands with a total area of 827.87 km^2. Jixi is located in the southeast of Heilongjiang Province, between 130°24′24″–°56′30″E, 44°51′12″–46°36′55″N. To the southeast and across the ocean in Russia, while to the west and south are Mudanjiang, and to the north is Qitaihe (Fig. 1). The province comprises Mishan, Hulin, and Jidong Counties and six other districts (Jiguan, Hengshan, Didao, Chengzihe, Lishu, and Mashan). The study area is part of the cold-temperate continental monsoon climate, where the average annual temperature is 3.7 °C, the average precipitation is 537.5 mm, the annual sunshine is 2709 h and the average frost-free period is 140 d. The terrain is composed primarily of mountains, hills and plains.

Jixi is relatively rich in mineral resources with mutiple mining areas. However, there also are several abandoned mines that severely damage the ecological environment. In addition, urban construction and industrial development have encroached on grasslands, woodlands, and wetlands, which increases the ecological vulnerability and risks in these ecosystems (*He, 2010*).

Data sources and preprocessing treatments

This paper is based on the Landsat 8 OLI remote sensing images from 2015 and 2019, all of which are from the US Geological Survey (http://glovis.usgs.gov/). All images have a spatial resolution of 30 m. The image strip numbers/rows used in this study are 115/28 and 115/29, respectively, and the imaging time was from July to September. Cloud cover in these images was less than 2%, and they were interpreted and classified based on a series of preprocessing treatments, including radiation calibration, atmospheric correction, band synthesis and image cropping.

Analytical methods

The spatial differentiation characteristics of the LST in the Jiguan, Didao, and Chengzihe Districts of Jixi were used to identify heat islands and their influencing factors. We selected a single-window algorithm for inversion of the LSTs. These results were used to analyze the effects of the land-use type, vegetation coverage and coal mining activities on the spatial distribution of LSTs.

Determining land-use classification and vegetation coverage

Land use is the most direct manifestation of the interaction between human activities and the natural environment as it reflects this close relationship in both time and space

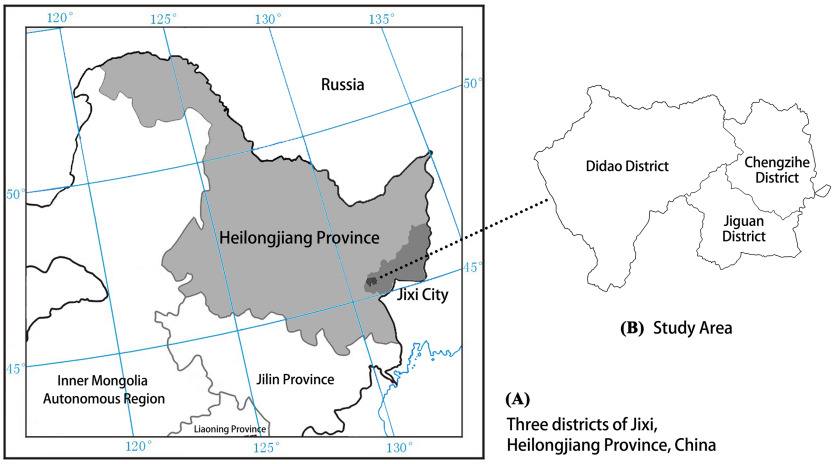

Figure 1 Location map showing the three districts of Jixi comprising the study area. Map representing the geostrategic importance of the study area: (A) Jixi City, Heilongjiang Province, China; (B) three districts of Jixi.

Full-size DOI: 10.7717/peerj.10257/fig-1

(*Mooney, Duraiappah & Larigauderie, 2013*; *Liu et al., 2014*). Typically, areas designated as land resources reflects the status of natural resources within the study area. Changes in land-use patterns inevitably cause changes in the LSTs and ecosystem functionality. Therefore, the study of land use is of great importance for regional ecological analyses (*Marceau et al., 2003*).

The relationship between vegetation coverage and the LST has become a focus of research on heat islands (*Wang et al., 2011*). Green vegetation affects LSTs through photosynthesis, transpiration and evapotranspiration. *Ma et al. (2010)* compared and analyzed five correlation degrees among planting parameters and LSTs, including the normalized difference vegetation index (NDVI), ratio vegetation index (RVI), greenness vegetation index (GVI), modified soil to adjust vegetation index (MSAVI) and vegetation coverage. They concluded that the correlation between vegetation coverage and the LST was both high and stable because it is not markedly influenced by spatial location or changes in the fraction or type of surface coverage. Therefore, the relationship between vegetation coverage and the LST was selected to study heat island effects within different land surfaces.

Land-use classification

The ENVI 5.3.1 (L3Harris Geospatial Solutions, Inc., Melbourne, FL, USA) and ArcGIS 10.5 (Esri, Corp., Redlands, CA, USA) were used to preprocess the original image data, which includes geometric correction, mosaic compilation, fusion, clipping, research scope extraction, image enhancement and supervised classification, before interpreting and analyzing the remote sensing imagery. The classification of land-use types in the study area was consistent with the standard land-use classification (GB/T 21010–2017). The study area was divided into six categories: forest lands, grasslands, construction lands, cultivated lands, mining lands and water areas. A maximum-likelihood approach was used for the

classification. In the final stage of the study, the remote sensing image interpretation was validated by site surveys. The accuracy of the results was verified by establishing a confusion matrix. Random points were selected in the Erdas Imagine 2015 software for classification, where a certain number of random points were selected for each category. The classification of each random point was distinguished visually so that the category to which each random point belongs is defined in the software. The user accuracy, producer accuracy, and Kappa coefficient of the overall classification of each category were then calculated.

Vegetation coverage calculation

Plant coverage information is typically extracted from remote sensing images. Given the high accuracy of NDVI values estimated using remote sensing, it is one of the most widely used indexes (*Mu et al., 2012*). A common method to calculate vegetation coverage is based on the hybrid pixel decomposition method, where it is assumed that each pixel of the remote sensing image is composed of soil and vegetation components. Thus, the information includes both a pure soil component and a pure vegetation component. In this case, we assumed that the NDVI value is a weighted average sum of the index values from both soil and vegetation information (*Li, Fan & Wang, 2010*), which is given as follows:

$$\mathrm{NDVI} = f_v \times \mathrm{NDVI}_{\mathrm{veg}} + \left(1 - f_v\right) \times \mathrm{NDVI}_{\mathrm{soil}}, \tag{1}$$

Where NDVI is the vegetation index value of mixed pixels; $\mathrm{NDVI}_{\mathrm{veg}}$ is the vegetation index of pure vegetation pixels; $\mathrm{NDVI}_{\mathrm{soil}}$ is the vegetation index value of pure soil pixels; and f_v is the vegetation coverage. Thus, the formula for vegetation coverage (f_v) becomes:

$$f_v = (\mathrm{NDVI} - \mathrm{NDVI}_{\mathrm{soil}}) / \left(\mathrm{NDVI}_{\mathrm{veg}} - \mathrm{NDVI}_{\mathrm{soil}}\right). \tag{2}$$

In practice, the parameters can be selected in the following ways. (1) Take different $\mathrm{NDVI}_{\mathrm{veg}}$ and $\mathrm{NDVI}_{\mathrm{soil}}$ values for different soil and vegetation types. (2) Use the maximum and minimum NDVIs of the study area, $\mathrm{NDVI}_{\mathrm{veg}} = \mathrm{NDVI}_{\mathrm{max}}$, $\mathrm{NDVI}_{\mathrm{soil}} = \mathrm{NDVI}_{\mathrm{min}}$. (3) Determine the NDVI value of the corresponding pixel based on measured data (*Li et al., 2015*). Under the influence of varying meteorological conditions, vegetation type and distribution, seasons, and other factors, both the $\mathrm{NDVI}_{\mathrm{soil}}$ and $\mathrm{NDVI}_{\mathrm{veg}}$ values for different images vary to some extent.

The maximum and minimum values of the given confidence interval are selected, and the confidence value is determined primarily from the image size and clarity. As a comparison, the maximum NDVI images of 2015 and 2019 were extracted. In the NDVI frequency accumulation table, the NDVI with a frequency of 5% was selected for $\mathrm{NDVI}_{\mathrm{soil}}$, and the NDVI with a frequency of 95% was selected for $\mathrm{NDVI}_{\mathrm{veg}}$. Finally, the vegetation coverage was obtained from Eq. (2).

Land surface temperature inversion

The LST inversion algorithms for single-infrared-band Landsat 8 OLI remote sensing data are based primary on the radioactive transfer equation (RTE), a universal single-channel algorithm, and a single-window algorithm (*Ding & Xu, 2008*). Therefore, the RTE was selected to invert the LSTs in this study.

Calculation of specific surface emissivity

Remote sensing images were firstly classified into three types: water bodies, towns and natural surfaces. The specific emissivity of water pixels is 0.995, where other surface emissivity estimates were based on the following formulas (*Chi, Zeng & Wang, 2016*):

$$\varepsilon_{\text{surface}} = 0.9625 + 0.0614 f_v - 0.0461 f_v^2 \tag{3}$$

$$\varepsilon_{\text{building}} = 0.9589 + 0.086 f_v - 0.0671 f_v^2 \tag{4}$$

Where $\varepsilon_{\text{surface}}$ and $\varepsilon_{\text{building}}$ represent the specific emissivity of natural surface pixels and urban pixels, respectively.

Radioactive transfer equation

The RTE is also called the atmospheric correction method. It firstly estimates the impact of the atmosphere on the surface thermal radiation based on the information received by the satellite thermal infrared sensor. This is then subtracted from the total thermal radiation obtained by the sensor. The impact of the atmosphere on the surface can be used to obtain the intensity of surface thermal radiation. Assuming that the surface and the atmosphere have Lambertian properties for thermal radiation, the corresponding LST can be obtained as (*You & Yan, 2009*; *Yue et al., 2019*):

$$L_\lambda = \left[\varepsilon \cdot B(T_S) + (1-\varepsilon) L_\downarrow\right] \cdot \tau + L_\uparrow, \tag{5}$$

Where L_λ is the intensity of thermal radiation received by the satellite sensor, ε(K) is the surface emissivity, T_S is the true LST, B(T_S) (W m^{-2} sr^{-1} μm^{-1}) is the black body brightness corresponding to temperature T_S derived from Planck's law, τ is the transmittance of the atmosphere at thermal infrared wavelengths, $L_\uparrow$ (W m^{-2} sr^{-1} μm^{-1}) is the atmospheric upward radiance, and $L_\downarrow$(W m^{-2} sr^{-1} μm^{-1}) is the atmospheric downward radiance. Based on the RTE, the B(T_S) can be obtained as (*Wu et al., 2016*; *Hou & Zhang, 2019*):

$$B(T_S) = \left[L_\lambda - L_\uparrow - \tau \cdot (1-\varepsilon) L_\downarrow\right] / \tau \cdot \varepsilon, \tag{6}$$

Where τ, $L_\uparrow$ (W m^{-2} sr^{-1} μm^{-1}) and $L_\downarrow$(W m^{-2} sr^{-1} μm^{-1}) were determined from the official NASA website (http://atmcorr.gsfc.nasa.gov/) by inputting the imaging time, latitude and longitude, air pressure and other relevant information to the study area. After estimating the of black body radiance B(T_S), which is the same as the real temperature on the ground, the inverse function of Planck's law gives the real temperature on the ground as (*Chen, 2014*):

$$T_S = K_2 / ln\left(\frac{K_1}{B(T_S)} + 1\right), \tag{7}$$

Where K_1 and K_2 are constants obtained by querying the Landsat metadata file. In this case, $K_1 = 774.8853$ and $K_2 = 1321.0789$ for Landsat 8 TIRS band 10.

Normalized temperature index and temperature classification

The ecological environment of coal mining areas is damaged to varying degrees, this changes their LSTs and causes a series of significant ecological effects and environmental problems, such as vegetation degradation and soil erosion (*Dutta & Agrawal, 2003*; *Zhou & Zhang, 2005*). We used the urban heat island effect to explore the impact of coal mining activities on LSTs (*Ye et al., 2011*; *Li et al., 2019*). The formula for the normalized temperature index is:

$$T_r = \frac{\Delta T}{T_{\text{range}}} = \frac{T - T_{\min}}{T_{\max} - T_{\min}}, \tag{8}$$

Where T_r is the normalized temperature index, T is the temperature at any spatial position in the region, $T_{\max}$ and $T_{\min}$ are the highest and lowest temperature in the region, respectively.

The method of equal intervals is used to divide the temperature based on the site conditions and existing research (*Sheng et al., 2010*; *Jia & Liu, 2006*). Once the maximum and minimum values of the inversion temperature are taken as endpoints, the temperature is divided into five equal-spaced intervals. These are a low-temperature zone, a low-middle-temperature zone, a middle-temperature zone, a middle-high-temperature zone, and a high-temperature zone. The normalized temperature indices for these levels were 0.0–0.2, 0.2–0.4, 0.4–0.6, 0.6–0.8, and 0.8–1.0, respectively (Table 1). Analyzing changes in the LST index at different distances from the mine allows evaluating the intensity and range of the heat island effect as caused by coal-mining activities.

Analytical method of factors affecting land surface temperature

The terrain over the study area is relatively flat, which facilitates farming, town construction, and coal mining activities. We analyzed the spatial differentiation of LSTs in this area, which was linked to land use, vegetation coverage and coal mining activities.

The influence of land-use classification on land surface temperature

The area and proportion of different types of land use were counted separately. Subsequently, the land-use and the LST maps were superimposed to obtain statistical data on the LSTs of various land-use types.

The influence of vegetation coverage on land surface temperature

A profile analysis more intuitively reflected the relationship between changes in LST and vegetation coverage at a given geographical location. Using the interpolation line function in ArcGIS 10.5 to view profile values of LST and vegetation coverage from 2015 and 2019 to compare and analyze their associated changes along profiles to evaluate the relationships between these variables.

The influence of coal mining activities on land surface temperature

The influence of patch area

Firstly, all mining areas within a distance of 1,500 m from the edge of the study area were screened. These selected mining area patches were then counted and grouped based on area. We then combined these data with our LST inversion to determine the maximum,

Table 1 The relationship between the normalized temperature index values and assigned temperature grades.

Normalized temperature index	Temperature grade
0.0–0.2	Low temperature zone
0.2–0.4	Low-middle temperature zone
0.4–0.6	Middle temperature zone
0.6–0.8	Middle-high temperature zone
0.8–1.0	High temperature zone

minimum, and average LSTs for different patches. Finally, the influence of these mining land patches on the LSTs were evaluated.

The influence of buffer range

Buffers with a range of 100–1,500 m at intervals of 100 m were set for each of the patches. The average LST in each buffer zone was extracted, and the trends in the LSTs at varying distances from the mining area were analyzed.

RESULTS

Land surface temperature inversion

The LST results for the Jiguan, Didao and Chengzihe Districts of Jixi in 2015 and 2019 are shown in Fig. 2 and Table 2. The temperatures in 2015 were in general higher than those in 2019. The average LST over the entire study area was 25.64 °C in 2015 and 22.10 °C in 2019. There is a similarity in the spatial distribution patterns of their LSTs. High temperatures are concentrated in the south-central and southeast parts of the study area, while the temperatures in the west and north are relatively low. In these two years, the average LST in the Jiguan District was higher than averages in the other two districts, but its highest temperature was lower than the maximum recorded in the Didao and Chengzihe Districts. The highest temperatures over the entire study area were 42.29 °C, which was recorded at Shenghe Coal Mine in the Didao District. Likewise, the highest temperature in the Chengzihe District was recorded at Chengshan Coal Mine. Thus, mining areas had much higher LSTs than average. While only two years were selected for the analysis, similar results validate the conclusions.

The LSTs from 2015 and 2019 were normalized and divided into five levels, as shown in Fig. 3 and Table 3. The LSTs in the study area were assigned primarily to the low-temperature, low-middle-temperature, and middle-temperature zones, which covered the LST range of 19.16–33.04 °C in 2015 and 16.29–29.37 °C in 2019. Among them, the low-middle-temperature zone had the largest area as it accounted for more than 70% of the total study area. The high-temperature and middle-high-temperature zones had smaller areas. The high-temperature zone was distributed primarily within the Didao and Chengzihe Districts. The Shenghe Coal Mine accounted for 53.08% of the total area of the high-temperature zone in 2015 and rose to 59.04% in 2019. The proportion of the Chengshan Coal Mine in the total area of the high-temperature zone increased from

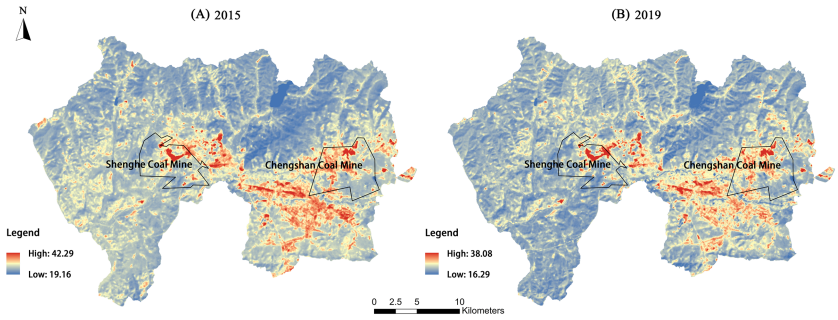

Figure 2 Land surface temperature (°C) results for the three districts of Jixi in 2019. Land surface temperature (LST) maps for (A) 2015, (B) 2019 of the three districts in Jixi, Heilongjiang, China.
Full-size DOI: 10.7717/peerj.10257/fig-2

Table 2 Statistics on LST for the study area in 2015 and 2019.

Range	Land surface temperature/°C							
	2015				2019			
	MEAN	MIN	MAX	STD	MEAN	MIN	MAX	STD
Jiguan District	27.16	21.58	38.97	2.52	23.24	17.42	33.64	2.23
Didao District	25.23	19.16	42.29	1.92	21.75	17.18	38.08	1.63
Chengzihe District	25.53	19.45	39.13	2.48	22.34	16.29	35.26	2.14
Total	25.64	19.16	42.29	2.28	22.10	16.29	38.08	1.95

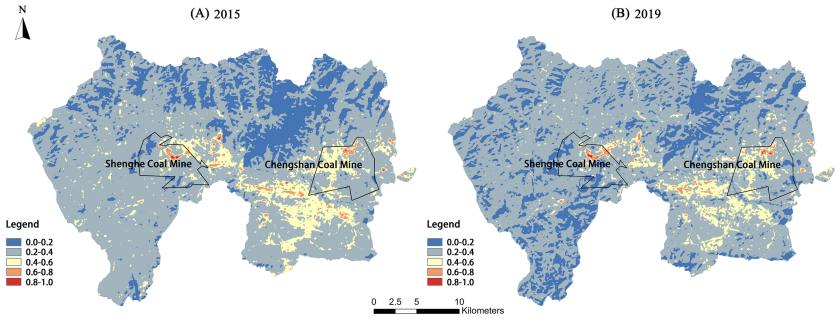

Figure 3 Spatial distribution of land surface temperature levels of the study area in 2015 and 2019. Spatial distribution of land surface temperature levels for (A) 2015, (B) 2019 of the three districts in Jixi, Heilongjiang, China.
Full-size DOI: 10.7717/peerj.10257/fig-3

8.17% to 34.47% over these four years. Meanwhile, the low-temperature and low-middle-temperature zones were distributed mostly in the Didao and Chengzihe Districts, giving a large temperature difference between them. Therefore, local heat island effects were obvious within the study area.

Land-use classification

Land-use types in the Jiguan, Didao, and Chengzihe Districts of Jixi in 2015 and 2019 are shown in Fig. 4 and Table 4. From 2015 to 2019, the area of forest land increased while

Table 3 LST normalization results for the study area in 2015 and 2019.

Temperature grade	Normalized temperature index	2015		2019	
		LST /°C	Percentage	LST /°C	Percentage
Low temperature zone	0.0–0.2	19.16–23.78	18.19%	16.29–20.65	19.31%
Low-middle temperature zone	0.2–0.4	23.78–28.41	70.53%	20.65–25.01	72.21%
Middle temperature zone	0.4–0.6	28.41–33.04	10.34%	25.01–29.37	7.79%
Middle-high temperature zone	0.6–0.8	33.04–37.66	0.90%	29.37–33.72	0.66%
High temperature zone	0.8–1.0	37.66–42.29	0.04%	33.72–38.08	0.03%
Total	0.0–1.0	19.16–42.29	100.00%	16.29–38.08	100.00%

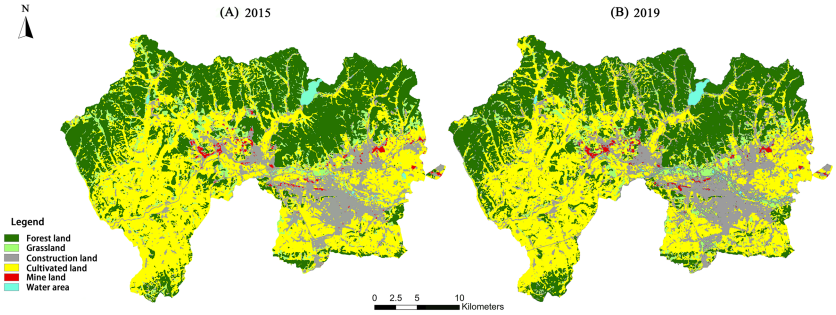

Figure 4 **Land-use types of the study area in 2015 and 2019.** Land-use types for (A) 2015, (B) 2019 of the three districts in Jixi, Heilongjiang, China.

Full-size DOI: 10.7717/peerj.10257/fig-4

the area of cultivated land decreased. However, the dominant land-use types in the study area are still forest land and cultivated land. The forest land is distributed mostly in the northern part of the study area, while the cultivated land is distributed in the middle and southern parts. Construction land is concentrated in the Jiguan District, which increased significantly from 109.94 km^2 to 133.69 km^2 in the four considered years. The mining land is defined primarily by the Shenghe Coal Mine in the Didao District and the Chengshan Coal Mine in the Chengzihe District. The accuracy of the land-use classification was verified by establishing a confusion matrix. The matrix showed that the Kappa coefficients of the land-use maps in the interpreted periods are all above 0.8, which meets the accuracy requirements for this study (Table 5).

Vegetation coverage

The remote sensing images of the study area were processed according to the mixed pixel decomposition method to obtain the vegetation coverage of the Jiguan, Didao, and Chengzihe District of Jixi (Fig. 5). The construction land in the eastern Jiguan District, Shenghe Coal Mine in the Didao District and Chengshan Coal Mine in the Chengzihe District had the lowest vegetation coverage. However, ongoing urbanization and coal mining activities have markedly affected vegetation coverage in many other areas as well.

Table 4 Land-use structure for the study area in 2015 and 2019.

Land-use	2015		2019	
	Area / km²	Percentage / %	Area / km²	Percentage / %
Forest land	294.07	35.52%	304.18	36.74%
Grassland	52.95	6.39%	80.4	9.71%
Construction land	109.94	13.28%	133.69	16.15%
Cultivated land	357.39	43.17%	295.07	35.64%
Mining land	7.10	0.86%	6.76	0.82%
Water area	6.42	0.78%	7.77	0.94%
Total	827.87	100.00%	827.87	100.00%

Table 5 Accuracy evaluation of land use classification for the study area in 2015 and 2019.

Land-use	2015						
	Forest land	Grassland	Construction land	Cultivated land	Mining land	Water area	Total
Forest land	1,646	2	–	–	–	–	1,648
Grassland	–	150	–	–	–	–	150
Construction land	3	–	2406	–	–	–	2,409
Cultivated land	–	4	2	1737	–	–	1,743
Mining land	–	–	17	–	346	–	363
Water area	–	–	–	–	–	319	319
Total	1649	156	2425	1737	346	319	6,632
Producers Accuracy	99.82	96.15	99.22	1000	100	98.46	–
Users Accuracy	99.88	100	99.67	99.66	95.32	100	–
				2019			
Forest land	858	35	–	–	–	–	893
Grassland	–	37	34	10	1	–	82
Construction land	–	–	1710	35	18	–	1,763
Cultivated land	2	11	19	821	2	–	855
Mining land	–	–	2	–	263	–	265
Water area	–	–	–	–	–	231	231
Total	860	83	1765	866	284	231	4,089
Producers Accuracy	99.77	44.58	96.88	94.8	92.61	92.4	–
Users Accuracy	96.08	45.12	96.07	95.8	99.25	100	–

Notes.

In 2015, Overall Classification Accuracy = 99.50%; Overall Kappa Statistics = 0.9932; In 2019, Overall Classification Accuracy = 95.42%; Overall Kappa Statistics = 0.9361.

Correlation between land surface temperature and land-use types

The main land types in the low-temperature and low-middle-temperature zone are water areas, forest land, grassland and cultivated land. The main land types in the high-temperature, middle-high-temperature, and middle-temperature zones are construction land and mining land. There are large difference in the average LSTs among these land-use types (Table 6). The average LSTs for mining land, construction land and grassland were higher than the average LST for the study area. Among them, mining land had the highest average LSTs (33.33 °C in 2015 and 29.63 °C in 2019), yielding temperature anomalies of

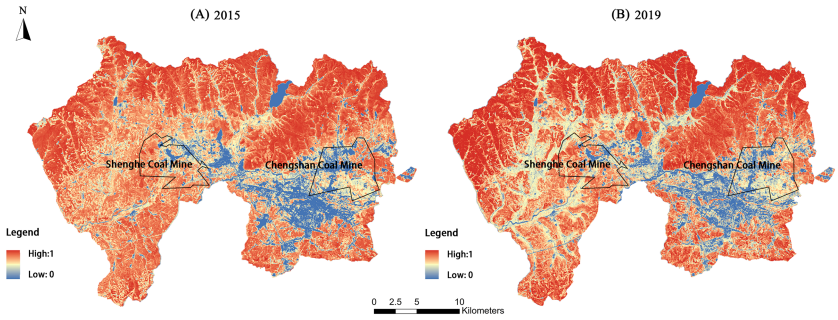

Figure 5 Vegetation coverage of the study area in 2015 and 2019. Vegetation coverage for (A) 2015, (B) 2019 of the three districts in Jixi, Heilongjiang, China.

Full-size DOI: 10.7717/peerj.10257/fig-5

Table 6 Statistics on LST of different land-use types in 2015 and 2019.

Land use types	Land surface temperature/°C							
	2015				2019			
	MEAN	MIN	MAX	STD	MEAN	MIN	MAX	STD
Forest land	23.95	20.79	30.89	1.01	21.07	17.38	26.41	0.97
Grassland	26.55	21.94	36.27	1.45	23.21	18.77	30.56	1.43
Construction land	29.12	20.59	41.74	2.26	24.62	17.24	35.04	1.96
Cultivated land	25.74	21.35	33.71	1.20	21.73	18.26	29.14	1.09
Mining land	33.33	24.27	42.29	2.50	29.63	20.35	38.08	2.31
Water area	21.72	19.16	29.12	2.30	19.31	16.29	27.56	1.74

7.69 °C in 2015 and 7.53 °C in 2019. The water area had the lowest average LSTs (21.72 °C in 2015 and 19.31 °C in 2019). At the same time, the temperature standard deviation within the mining land was also relatively large, with a difference of 18.02 °C between the minimum and maximum temperatures.

Correlation between land surface temperature and vegetation coverage

An east–west transect was drawn across the study are, and the data from 2019 were used to analyze changes in the LSTs with vegetation coverage. Every 25 pixel points on the profile were assigned to a group, and the average value of the vegetation coverage and LST in each group was calculated to obtain 56 data sets. Finally, a linear fit was performed between the vegetation coverage and average LST, and the coefficient of determination was assessed (Fig. 6). Areas with low vegetation coverage were associated with higher LSTs. In addition, as vegetation coverage decreased, the LSTs increased. The trends in LST and vegetation coverage were opposite with reciprocal change patterns.

The linear fit of the average LST and vegetation coverage (Fig. 7) shows that if the vegetation coverage increases by 0.1, the average LST is expected to decrease by approximately 0.75 °C. This constitutes a strong negative relationship between the LST and vegetation coverage. Using the SPSS 24 (IBM, Corp., Armonk, NY, USA) indicated a

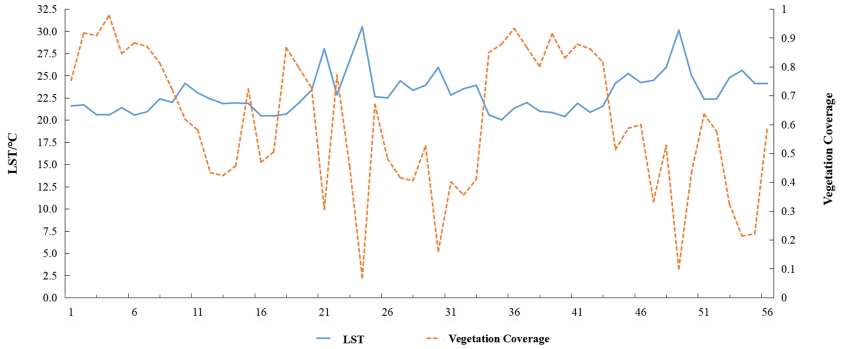

Figure 6 **Variation in land surface temperature (LST) and vegetation coverage in pixel groups (1–56) along an E-W profile.**

Full-size DOI: 10.7717/peerj.10257/fig-6

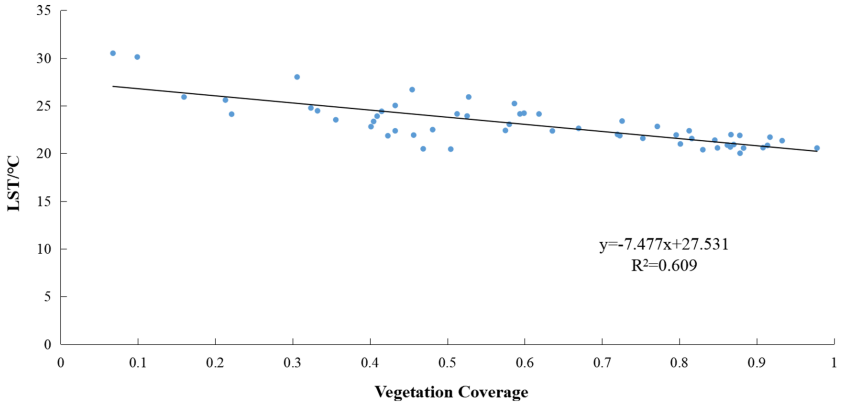

Figure 7 **Correlation between land surface temperature (LST) and vegetation coverage of the study area.**

Full-size DOI: 10.7717/peerj.10257/fig-7

correlation coefficient of $R = -0.780$. This indicates a significant correlation at the 0.01 confidence level (both sides). Thus, green vegetation has a significant cooling effect on the land surface.

Correlation between land surface temperature and coal mining activities

This study mainly considers spatial variations when exploring the correlation between the LST and mining activities. Therefore, the data of the most recent year (2019) is selected for the analysis, and the spatial distribution of the LST is analyzed based on the patch area and buffer sizes.

Correlation between land surface temperature and patch area of mining lands

The mining areas were grouped based on patch area after screening them within 1500 m of the edge of the study area. The maximum, minimum and average LSTs of each patch were calculated from the 52 data sets (Table 7). Correlations among the average patch area and

Table 7 Statistics on LST and patch area for mining lands.

Average area /m²	LST/°C		Average area /m²	LST/°C		Average area /m²	LST/°C	
	MEAN	MAX		MEAN	MAX		MEAN	MAX
900	26.88	30.98	**18000**	29.09	30.27	**53100**	30.22	31.95
1800	27.38	32.30	**19800**	29.17	35.11	**58500**	27.85	29.48
2700	27.25	30.87	**20700**	31.85	33.43	**61200**	29.79	31.73
3600	26.50	30.49	**21600**	29.60	30.61	**65700**	31.90	34.51
4500	27.97	31.39	**23400**	29.29	30.25	**82800**	30.79	32.06
5400	28.23	30.16	**24300**	28.47	31.40	**88200**	29.63	31.78
6300	27.46	31.61	**25200**	29.02	30.51	**110700**	28.62	30.18
7200	27.26	30.87	**26100**	27.89	29.30	**114300**	31.36	33.22
8100	26.52	29.54	**27000**	28.26	29.43	**135000**	28.94	31.05
9000	27.57	29.63	**28800**	28.59	31.25	**139500**	28.70	31.22
9900	28.39	30.63	**31500**	27.54	30.19	**162000**	29.85	32.49
10800	28.23	31.98	**32400**	28.33	31.92	**175500**	30.14	32.31
12600	28.26	33.02	**36000**	28.48	30.26	**179100**	30.13	32.35
13500	29.44	30.58	**39600**	28.54	30.53	**241200**	29.04	31.41
14400	26.99	29.11	**40500**	27.86	30.36	**490500**	31.15	33.10
15300	25.58	26.63	**43200**	28.33	30.66	**626400**	31.58	35.26
16200	27.53	28.46	**48600**	29.85	31.84	**754200**	31.58	38.08
17100	26.57	29.39						

the average and maximum patch temperatures were analyzed using SPSS 24. Our analysis indicates that the patch was strongly positively correlated with the average and maximum patch temperatures.

Correlation between the patch area and average patch temperature (Fig. 8) yielded $R = 0.571$. This indicates a significant correlation at the 0.01 confidence level (both sides). The determination coefficient of the fit logarithmic function was $R^2 = 0.487$, indicating that larger patch sizes promote a greater average patch temperature. Within 200,000 m^2, the average patch temperature increases rapidly with the size of the patch area. Once above 200,000 m^2, the average patch temperature increases more slowly.

The correlation between the patch area and maximum patch temperature (Fig. 9) yielded $R = 0.645$. This indicates a significant correlation at the 0.01 confidence level (both sides). The determination coefficient of the linear fit was $R^2 = 0.415$, indicating that larger patch sizes promote a greater maximum patch temperature. If the patch area of mining land increases by 100,000 m^2, the maximum patch temperature will increase by approximately 0.81 °C.

Correlation between land surface temperature and various buffer sizes

The schematic diagram of buffer zone in mining land patch is shown in Fig. 10. A correlation analysis was performed on average patch area, average patch temperature, maximum patch temperature of mining land and the average LST in buffer zones at 100–1,500 m reviewed at 100 m intervals (Table 8). The temperature of the buffer zones within 0–100 m was strongly correlated with the patch area, average patch temperature, and maximum patch

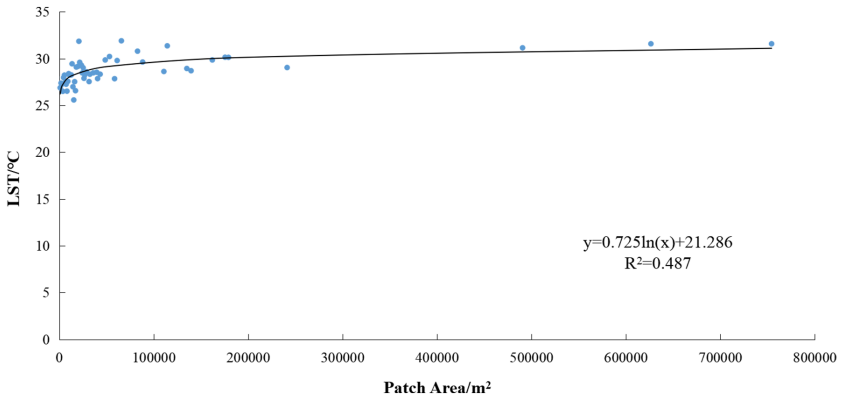

Figure 8 Correlation between patch area and average patch temperature of mining lands. LST, land surface temperature.

Full-size DOI: 10.7717/peerj.10257/fig-8

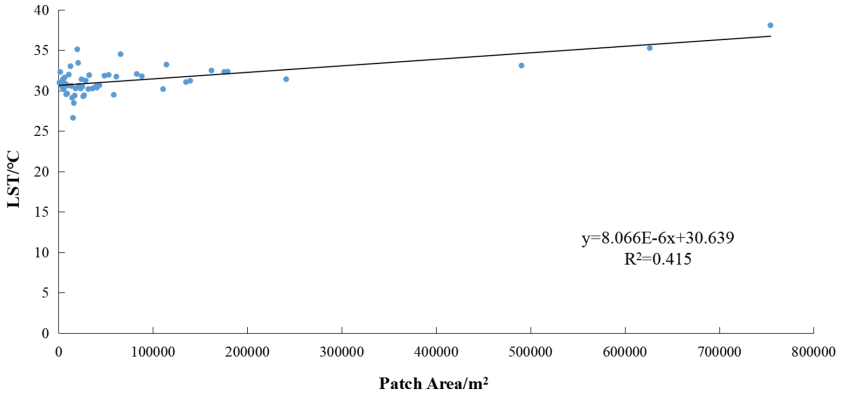

Figure 9 Correlation between patch area and maximum patch temperature of mining lands. LST, land surface temperature.

Full-size DOI: 10.7717/peerj.10257/fig-9

temperature of the mining land. In the 100–200 m buffer zone, the correlation between the temperature and the average area was not significant. Therefore, a higher correlation was found for the entire buffer zone with the average and maximum patch temperatures, while a lower correlation was found with the patch area. Thus, the correlation between the temperature in the buffer zone and the average patch temperature was most relevant.

To further study the correspondence between the average patch temperature of mining land and the temperature in the buffer zones, the 52 data sets were sorted based on their average patch temperatures from smallest to largest. Each of the 13 groups was then compiled into a new group. The average number and the average temperature of the corresponding buffer zone in each new group were calculated to obtain four new data sets (Table 9).

Figure 11 shows that the further the buffer zone was from the mine land patch, the lower its temperature. In 0–200 m buffer zones, the average temperature changed drastically, while the average temperature outside the 200 m zone varied little. The range of this heating

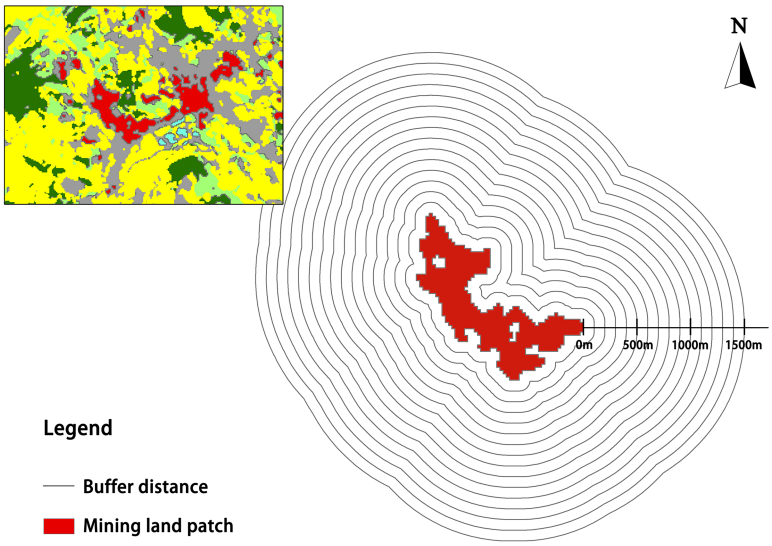

Figure 10 Schematic diagram of buffer zone in mining land patch. The key has been noted in the figure.
Full-size DOI: 10.7717/peerj.10257/fig-10

Table 8 Correlation between LST and buffer zone within the mining lands.

Factor		Average area	Average temperature	Maximum temperature
Average temperature in buffer zone / °C	100 m	0.35**	0.79**	0.71**
	200 m	0.07	0.41**	0.39**
	300 m	−0.01	0.31*	0.26
	400 m	−0.03	0.30*	0.25
	500 m	0.01	0.33*	0.30*
	600 m	0.02	0.33*	0.28*
	700 m	0.03	0.30*	0.27
	800 m	0.05	0.28*	0.28*
	900 m	0.09	0.28*	0.30*
	1,000 m	0.09	0.29*	0.29*
	1,100 m	0.09	0.29*	0.28*
	1,200 m	0.12	0.33*	0.30*
	1,300 m	0.10	0.32*	0.27
	1,400 m	0.08	0.29*	0.24
	1,500 m	0.10	0.28*	0.26

Notes.
*$p < 0.05$.
**$p < 0.01$.

effect is approximately 700 m in Group 1, 1,200 m in Group 2 and 3, and more than 1,400 m in Group 4. Therefore, a larger average patch temperature in the mining land causes a higher temperature in its buffer zone, and the greater the scope of its influence.

Table 9 Correspondence between LST and buffer zone within the mining lands.

Average Temperature/°C		27.00	28.20	29.05	30.78
Average temperature in different scale buffers /° C	100 m	25.15	25.84	26.01	27.17
	200 m	24.39	24.75	24.43	25.36
	300 m	24.34	24.65	24.16	25.11
	400 m	24.22	24.64	24.07	25.00
	500 m	24.06	24.69	24.04	24.97
	600 m	23.87	24.63	24.12	24.78
	700 m	23.76	24.53	24.14	24.59
	800 m	23.70	24.44	23.95	24.52
	900 m	23.64	24.24	23.80	24.47
	1,000 m	23.59	24.06	23.77	24.41
	1,100 m	23.54	23.87	23.72	24.29
	1,200 m	23.48	23.68	23.71	24.21
	1,300 m	23.43	23.57	23.68	24.07
	1,400 m	23.43	23.55	23.66	23.96
	1,500 m	23.42	23.52	23.51	23.92

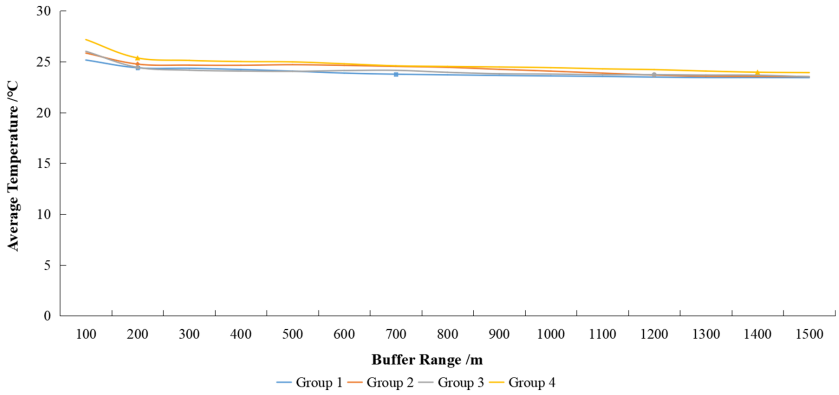

Figure 11 **Variation of land surface temperature (LST) with buffer zone of mining lands.** The double line on the coordinate axis represents the omitted part of the value, so the *Y*-axis can more clearly reflect the trend of the four sets of data in the figure.

Full-size DOI: 10.7717/peerj.10257/fig-11

DISCUSSION

Impact of coal mining activities on surface temperatures

As the largest coal city in Heilongjiang Province, Jixi has always utilized coal as its leading industry. The main types of coal mining wasteland in Jixi City include mining subsidence, land occupation, polluted wasteland, and excavated land, which account for 0.48%, 82.0%, 6.82%, and 10.71% of the total coal mining wasteland, respectively (*Di, Guan & Zheng, 2015*). Coal mining activities generate a significant amount of heat. Thus, regional heating within the city has intensified when coupled with their high-energy consumption and high-heat producing enterprises (*Hu, Zhao & Dong, 2010*). The ongoing economic development

of mining areas has increased both the population density and heat production from urban infrastructure.

The correlation between LST and coal mining activities has resulted in larger mining lands with higher average and maximum patch temperatures. The available literature has shown that the size, shape, number, and boundary properties of these patches affect their energy transmissions. According to landscape ecological theory, the size and shape of these patches also affect their energy accumulation. Likewise, some researchers have recognized that larger patches of construction land have higher degrees of aggregation, more regular shapes, higher LSTs, and more significant heat island effects (*Yu, 2006*; *Fu, 2001*; *Xie, Wang & Fu, 2011*; *Xu et al., 2015*). Some studies have analyzed different types of disturbances at the interior of mining lands, among which dumps, opencast coal pits, and industrial centers have higher contributions to local warming (*Xie, Wang & Fu, 2011*; *Liu, 2016*). Exposed coal and coal gangue easily absorb heat and cause increased temperatures, while piled coal gangue hills are prone to heat and spontaneous combustion (*Hao, 2011*). Therefore, many factors cause high temperatures in mining land.

Quantitative research on the impact of mining land indicates a strong warming effect within a buffer zone of 0–200 m around mining land patches. As the distance from the mining land increases, the warming effects gradually weakens. Mining land patches with higher average patch temperatures have larger temperature-affected buffer zones. Changes in the local meteorological conditions, such as temperature rise, affect local species, which impacts the ecological conditions of the entire region. However, the strength of the warming effect and the size of its influence range are not only related to the distance from the mining land patch but may also be related to the average temperature of the entire area during the analysis (*Liao, 2009*). This specific correlation requires further study.

To date, regulations on the ecological and environmental protection are aimed only at the ecological and environmental indicators within the mining area, which cannot achieve regional ecological protection. Although it seems intuitive that coal production enterprises or units engaged in corresponding activities have taken the responsibility of protecting the ecology and environment, this does not cover the entire affected area of coal mining production activities. To protect the ecological quality of the area while developing coal resources, the scope of environmental protection in mining areas should be defined more scientifically and rationally.

Impact of different land-use types on surface temperature

Our results show that land-use types have a dominating impact on the LST. The LSTs of the Jiguan, Didao, and Chengzihe District of Jixi were primarily within the range of 16.29–42.29 °C in the two considered years. The low-middle-temperature zone had the largest area, which accounted for 70.53% and 72.21% of the total area. The low-temperature zone was distributed primarily over water areas, forest lands and cultivated lands. The high-temperature zone was distributed mostly over the construction land and mining land, especially the Shenghe Coal Mine in the Didao District and the Chengshan Coal Mine in the Chengzihe District.

The temperatures in 2019 were generally lower than those in 2015. From a normalized comparison, it is seen that the high-temperature and low-temperature zones increased in 2019. Along with the clustered development of mining land patches, the land surface temperature shows a polarizing trend. The expansion of some high-temperature zones may be due to the continued development of coal mines. The increased low-temperature areas may be due to the reclamation and restoration of vegetation in mining areas. Based on governmental planning (''Mineral Resources Planning of Jixi City (2016-2020)'' and ''Special Planning for Reclamation and Utilization of Desert Land of Industrial Mining Area and Mining Subsidence Area in Jixi City (2014–2020)'') from 2015 to 2019, the coal industry wastelands in Chengzihe and Didao Districts were treated to a certain extent, and the reclaimed land was converted into cultivated land, forest land, and construction land. These lands will be used for agricultural production, creating recreational landscapes, and improving the ecological environment.

In recent years, the development of coal resources in Jixi has been rapid. Additionally, the spatial distribution of mines has also changed (*Yang, 2013*). Construction and mining activities have reduced the ''cooling'' land-use types, such as forest and cultivated lands (*Wang et al., 2020*), and replaced them with ''warming'' types, like construction and mining lands. The available literature has shown that urban expansion is the main driving process of land cover changes and consequently rise of LST (*Pal & Ziaul, 2017*), which is consistent with our findings. With changes in land-use types, natural vegetation has been replaced by impervious concrete and construction land, which has caused significant changes like heat radiation from the underlying city surface (*Wang et al., 2013*). These man-made surfaces have a strong light absorptive effect and can quickly raise the local LST (*Hien et al., 2011*). In addition, building facades can reflect light multiple times, heating the near-surface atmosphere and cause LSTs to rise significantly (*Miao et al., 2009*). Some studies have also shown that the heating effect of construction lands, especially compact low-rise buildings, is very obvious (*Das, Das & Mandal, 2020*). Among the six considered land-use types, the LSTs of water area, forest land, and cultivated land were lower than the average LST for the study area. Water-permeable areas of the study region, such as water areas and forest land, ensure efficient heat exchange between the soil and the atmosphere. Water can evaporate, which absorbs heat in the environment and has an overall cooling effect (*Zhang et al., 2013a*; *Zhang et al., 2013b*). Therefore, not only by balancing the land-use types, but also by optimizing appropriate urban planning, the increase in LST can be adjusted to reduce the impact of urbanization on the ecological environment (*Das & Das, 2020*).

Impact of vegetation coverage on land surface temperatures

Our coupling analysis showed that changes in vegetation coverage are very important factors that affecting ecological status change. There is a significant negative correlation between LST and vegetation coverage, which has also been confirmed by other works (*Estoque, Murayama & Myint, 2017*; *Jiang, Zeng & Zeng, 2015*; *Duan & Zhang, 2012*; *Wu, Xu & Tan, 2007*; *Yue, Xu & Xu, 2006*). As vegetation blocks sunlight, it reduces the amount of solar radiation that reaches the surface, while plant transpiration also reduces the LST (*Cui, Li & Ji, 2018*). In areas with high vegetation coverage, the LST was lower than in

other areas, illustrating the degree to which vegetation could effectively alleviate heat island effect.

Therefore, municipal bodies should carefully consider the balance between ecological protection and economic development. The focus should be on vegetation restoration and environmental governance in areas where heat emissions are concentrated, such as abandoned mine sites and barren areas. Meanwhile, increasing the proportion of green space, improving the diversity and complexity of the landscape, and dividing the impervious surface with vegetation when developing urban construction land and coal mines can significantly reduce the LST and alleviate heat island effects.

CONCLUSIONS

Our findings show that coal mining activities and urban expansion are the primary factors affecting LSTs. These two factors change land-use types and vegetation coverage, which results in an abnormal heat flux. There were large differences in the LSTs among the various land-use types in Jixi City. The LSTs for the considered land-use types were ranked from high to low, as follows: mining land > construction land > grassland > cultivated land > forest land > water area. The average LST difference between the mining land and water area was more than 10 °C each year.

Correlations between LST and vegetation coverage indicate that they have a significant negative relationship. The LST was lower in areas with higher vegetation coverage than in other areas. For every 0.1 increase in vegetation coverage, the surface temperature is expected to drop by approximately 0.75 °C, indicating the extent to which vegetation can effectively alleviate warming effects.

The correlation between the LST and coal mining activities indicates the patch area of the mining land has a significant positive correlation with both the average and maximum patch temperatures. The average patch temperature shows a logarithmic increase with the growth of the patch area; thus, the average patch temperature increases significantly within 200,000 m^2. The maximum patch temperature shows a linear increase with the growth of the patch area; thus, the maximum patch temperature increases by approximately 0.81 °C for every 100,000 m^2 increase in the patch area of mining land. A higher correlation was found between the average patch temperature and the temperature in the buffer zone. This study found that the higher the average patch temperature of mining land, the higher the temperature in its buffer zone, and the greater the scope of its influence. As the distance from the mining land increased, its heating effect weakened.

Full consideration should be given to vegetation restoration in mining areas to reduce the warming effect from coal mining activities, especially in abandoned mining land, by increasing the total vegetation coverage in the study area. The existing large coal mine land patches need to be divided by plants or water areas. Thus, the scope of environmental protection in mining areas needs to be correctly defined. Meanwhile, in future urban layouts, downtown areas should maintain a proper distance from coal mining land. This study provides a useful reference to explore the warming effects caused by coal mining activities and the definition of its influence scope.

ADDITIONAL INFORMATION AND DECLARATIONS

Funding

This work was supported by the Fundamental Research Funds for the Central Universities (No.2572017CA12, No.2572018CP06). The funders had no role in study design, data collection and analysis, decision to publish, or preparation of the manuscript.

Grant Disclosures

The following grant information was disclosed by the authors:
Fundamental Research Funds for the Central Universities: No.2572017CA12, No.2572018CP06.

Competing Interests

The authors declare there are no competing interests.

Author Contributions

- Jia-shuo Cao and Zheng-yu Deng conceived and designed the experiments, performed the experiments, analyzed the data, prepared figures and/or tables, authored or reviewed drafts of the paper, and approved the final draft.
- Wen Li conceived and designed the experiments, analyzed the data, authored or reviewed drafts of the paper, and approved the final draft.
- Yuan-dong Hu analyzed the data, authored or reviewed drafts of the paper, and approved the final draft.

Data Availability

The following information was supplied regarding data availability:

Data is available at Open Science Framework: Dengzhengyu. 2020. "Remote Sensing Inversion and Spatial Variation of Land Surface Temperature over Mining Areas of Jixi, Heilongjiang, China." OSF. November 3. https://osf.io/tj9wh/.

Supplemental Information

Supplemental information for this article can be found online at http://dx.doi.org/10.7717/peerj.10257#supplemental-information.

REFERENCES

Bian ZF, Lei SG, Jin D, Wang L. 2018. Several basic scientific issues related to mined land remediation. *Journal of China Coal Society* **43(1)**:190–197 DOI 10.13225/j.cnki.jccs.2017.4004.

Chabukdhara M, Singh OP. 2016. Coal mining in northeast India: an overview of environmental issues and treatment approaches. *International Journal of Coal Science & Technology* **3(2)**:87–96 DOI 10.1007/s40789-016-0126-1.

Chen Y. 2014. A preliminary study on the urban heat island effect based on Landsat 8: case of Xiamen City. *Geomatics & Spatial Information Technology* **37(2)**:123–128 DOI 10.3969/j.issn.1672-5867.2014.02.036.

Chi TL, Zeng J, Wang ST. 2016. Research of the relationship between vegetation fraction and evolution of thermal environment in Zhengzhou based on RS and GIS technology. *Chinese Landscape Architecture* **32(10)**:78–83.

Cui LL, Li GS, Ji DJ. 2018. Heat island effect and its relationship with land use in Chengdu City. *Chinese Journal of Ecology* **37(5)**:1518–1526 DOI 10.13292/j.1000-4890.201805.001.

Das M, Das A. 2020. Assessing the relationship between local climatic zones (LCZs) and land surface temperature (LST)—a case study of Sriniketan-Santiniketan Planning Area (SSPA), West Bengal, India. *Urban Climate* **32**:100591 DOI 10.1016/j.uclim.2020.100591.

Das M, Das A, Mandal S. 2020. Outdoor thermal comfort in different settings of a tropical planning region: a study on Sriniketan-Santiniketan Planning Area (SSPA), Eastern India. *Sustainable Cities and Society* **63**:102433 DOI 10.1016/j.scs.2020.102433.

Di C, Guan GF, Zheng H. 2015. Study on reclamation potential evaluation of abandoned land after coal mining in Jixi City. *Territory & Natural Resources Study* **1**:27–29 DOI 10.16202/j.cnki.tnrs.2015.01.009.

Ding F, Xu HQ. 2008. Comparison of three algorithms for retrieving land surface temperature from Landsat TM thermal infrared band. *Journal of Fujian Normal University (Natural Science Edition)* **99(1)**:91–96.

Duan JL, Zhang XL. 2012. Correlative analysls of the diversity patterns of regional surface water, NDVI and thermal environment. *Chinese Journal of Applied Ecology* **23(10)**:2812–2820 DOI 10.13287/j.1001-9332.2012.0400.

Dutta RK, Agrawal M. 2003. Restoration of opencast coal mine spoil by planting exotic tree species: a case study in dry tropical region. *Ecological Engineering* **21(2–3)**:143–151 DOI 10.1016/j.ecoleng.2003.10.002.

Estoque RC, Murayama Y, Myint SW. 2017. Effects of landscape composition and pattern on land surface temperature: an urban heat island study in the megacities of Southeast Asia. *Science of the Total Environment* **577**:349–359 DOI 10.1016/j.scitotenv.2016.10.195.

Fu BJ. 2001. *Principle and response of landscape ecology*. Beijing: Science Press.

Gan FP, Chen WT, Zhang XJ, Yan BK, Liu SW, Yang SM. 2006. The progress in the study of thermal infrared remote sensing for retrieving land surface temperature. *Remote Sensing for Land & Resources* **67**:6–11 DOI 10.3969/j.issn.1001-070X.2006.01.002.

Gillespie A, Rokugawa S, Matsunaga T, Cothern JS, Hook S, Kahle AB. 2002. A temperature and emissivity separation algorithm for Advanced Spaceborne Thermal Emission and Reflection Radiometer (ASTER) images. *IEEE Transactions on Geoscience & Remote Sensing* **36(4)**:1113–1126 DOI 10.1109/36.700995.

Hao YF. 2011. Research on the ecological restoration and ecological services of abanoned mine land in mountain regions. D. Thesis, China University of Mining and Technology.

He L. 2010. Synthetic evaluation of ecological environment influenee, ecological environmental protection and ecology repair countermeasures for open-pit mining. D. Thesis, Northwest University.

Hien WN, Kardinal JS, Samsudin R, Eliza A, Ignatius M. 2011. A climatic responsive urban planning model for high density city: Singapore's commercial district. *International Journal of Sustainable Building Technology and Urban Development* **2(4)**:323–330 DOI 10.5390/SUSB.2011.2.4.323.

Hou YC, Zhang DY. 2019. Comparison study on land surface temperature retrieval algorithms based on Landsat 8 remote sensing image. **35(10)**:142–147 DOI 10.11924/j.issn.1000-6850.casb18120100.

Hu ZQ, Duo LH, Wang XT. 2018. Principle and method of reclaiming subsidence land with inter-layers of filling materals. *Journal of China Coal Society* **43(1)**:198–206 DOI 10.13225/j.cnki.jccs.2017.4003.

Hu WL, Zhao P, Dong ZY. 2010. Thermal environment effect of coal mining area and its ecological significance based on TM data. *Journal of Hefei University of Technology (Natural Science)* **33(5)**:741–744.

Jia HF, Liu XH. 2006. *Principle and application of environmental remote sensing*. Beijing: Tsinghua University Press.

Jiang MZ, Zeng SP, Zeng J. 2015. Urban expansion of Tianjin and the micro climate characteristics evolution: based on the urban thermal environment perspective. *Journal of Arid Land Resources and Environment* **29(9)**:159–164 DOI 10.13448/j.cnki.jalre.2015.310.

Jiménez-Muñoz JC, Cristobal J, Sobrino JA, Soria G, Pons X. 2008. Revision of the single-channel algorithm for land surface temperature retrieval from Landsat thermal-infrared data. *IEEE Transactions on Geoscience & Remote Sensing* **47(1)**:339–349 DOI 10.1109/TGRS.2008.2007125.

Li HZ, Chen JS, Han Y, Zhang YN. 2019. Micro-scale research of the impact factors on urban thermal environment: a case study of Luohu District, Shenzhen. *Ecology and Environmental Sciences* **28(8)**:1622–1631 DOI 10.16258/j.cnki.1674-5906.2019.08.015.

Li ZL, Duan SB, Tang BH, Wu H, Ren HZ, Yan GJ, Tang RL, Leng P. 2016. Review of methods for land surface temperature derived from thermal infrared remotely sensed data. *Journal of Remote Sensing* **20(5)**:899–920 DOI 10.11834/jrs.20166192.

Li DK, Fan JZ, Wang J. 2010. Change characteristics and their causes of fractional vegetation coverage (FVC) in Shanxi Province. *Chinese Journal of Applied Ecology* **21(11)**:2896–2903 DOI 10.13287/j.1001-9332.2010.0404.

Li YW, Jia K, Wei XQ, Yao YJ, Sun J, Mou LQ. 2015. Fractional vegetation cover estimation in northern China and its change analysis. *Remote Sensing for Land and Resources* **27(2)**:112–117 DOI 10.6046/gtzyyg.2015.02.18.

Li J, Miao H, Yang Z, Han Y. 2018. Spatial variation of land surface temperature in Yanzhou coalfield. *Journal of China Coal Society* **43(9)**:2595–2604 DOI 10.13225/j.cnki.jccs.2018.0019.

Li RL, Shi YJ, Yao YM, Tian FP, Hu Y. 2014. Temporal and spatial variation of oasis cold island effect in Ganzhou district of Zhangye based on Landsat TM/ETM +. *Journal of Arid Land Resources and Environment* **28(9)**:139–144 DOI 10.13448/j.cnki.jalre.2014.09.012.

Li HK, Yang L, Lei J. 2017. Comparison of Landsat-8 thermal infrared data for retrieving land surface temperature in rare earth mining area. *Journal of the Chinese Rare Earth Society* **35(5)**:657–666 DOI 10.11785/S1000-4343.20170512.

Liang BP, Zhai LX. 2014. A research on spatial–temporal changes and correlation between vegetation fraction and land surface temperature in Guilin during 1991—2006. *Chinese Landscape Architecture* **30(7)**:77–81.

Liao CH. 2009. Study on ecological effects of mining landscape and ecological restoration in Yangquan coal mining region. M. Thesis, Tsinghua University.

Liu J. 2016. The research to the influential factors of the surface temperature in Antaibao Opencast Coal Mine. D. Thesis, China University of Geosciences.

Liu JY, Kuang WH, Zhang ZX, Xu XL, Qin YW, Ning J, Zhou WC, Zhang SW, Li RD, Yan CZ, Wu SX, Shi XZ, Jiang N, Yu DS, Pan XZ, Chi WF. 2014. Spatiotemporal characteristics, patterns and causes of land use changes in China since the late 1980s. *Acta Geographica Sinica* **69(1)**:3–14 DOI 10.11821/dlxb201401001.

Ma W, Zhao ZM, Liu X, Yan DC. 2010. A quantitative analysis of the relationship between vegetation indices and land surface temperature based on remote sensing: a case study of TM data for Beijing. *Remote Sensing for Land & Resources* **22(4)**:108–112 DOI 10.6046/gtzyyg.2010.04.22.

Mao KB, Qin ZH, Shi JC, Gong P. 2005. The research of split-window algorithm on the MODIS. *Geomaticss and Information Science of Wuhan University* **30(8)**:703–707 DOI 10.3321/j.issn:1671-8860.2005.08.011.

Marceau DJ, Howarth PJ, Dubois JM, Gratton DJ. 2003. Evaluation of the grey-level co-occurrence matrix method for land-cover classification using spot imagery. *IEEE Transactions on Geoscience and Remote Sensing* **28(4)**:513–519 DOI 10.1109/TGRS.1990.572937.

Miao S, Chen F, Lemone MA, Tewari M, Wang Y. 2009. An observational and modeling study of characteristics of urban heat island and boundary layer structures in Beijing. *Journal of Applied Meteorology and Climatology* **48(3)**:484–501 DOI 10.1175/2008JAMC1909.1.

Mooney HA, Duraiappah A, Larigauderie A. 2013. Evolution of natural and social science interactions in global change research programs. *Proceedings of the National Academy of Sciences of the United States of America* **110**:3665–3672 DOI 10.1073/pnas.1107484110.

Mu SJ, Li JL, Chen YZ, Gang CC, Zhou W, Ju WM. 2012. Spatial differences of variations of vegetation coverage in inner Mongolia during 2001–2010. *Acta Geographica Sinica* **67(9)**:1255–1268 DOI 10.11821/xb201209010.

Pal S, Ziaul S. 2017. Detection of land use and land cover change and land surface temperature in English Bazar urban centre. *The Egyptian Journal of Remote Sensing and Space Science* **20(1)**:125–145 DOI 10.1016/j.ejrs.2016.11.003.

Pan DL, Huang ZQ, Zhang DR, Wang J, Zhou LF. 2013. Mapping land subsidence related to underground coal fires in the Wuda Coalfield (Northern China) using a small stack of ALOS PALSAR differential interferograms. *Remote Sensing* **5(3)**:1152–1176 DOI 10.3390/rs5031152.

Qin ZH, Karnieli A. 2001. A split window algorithm for calcu-lating land surface temperature using NOAA-AVHRR thermal channel data. *Remote Sensing for Land & Resources* **2**:33–42 DOI 10.3969/j.issn.1001-070X.2001.02.007.

Qin ZH, Karnieli A, Berliner P. 2001. A mono-window algorithm for retrieving land surface temperature from Landsat TM data and its application to the Israel-Egypt border region. *International Journal of Remote Sensing* **22(18)**:3719–3746 DOI 10.1080/01431160010006971.

Qiu WW, Hou HP. 2013. Study on surface temperature variation caused by ecological disturbance in the mining area based on RS. *Mining Research and Development* **33(2)**:68–71 DOI 10.13827/j.cnki.kyyk.2013.02.003.

Rozenstein O, Qin ZH, Derimian Y, Karnieli A. 2014. Derivation of land surface temperature for Landsat -8 TIRS using a split window algorithm. *Sensors* **14(4)**:5768–5780 DOI 10.3390/s140405768.

Sheng H, Wan H, Cui JY, Guo P. 2010. Urban heat island effect study and pridiction analysis based on Landsat TM data. *Remote Sensing Technology and application* **25(1)**:8–14 DOI 10.1080/00927872.2012.701681.

Wang RC, Hou H, Murayama Y, Derdouri A. 2020. Spatiotemporal analysis of land use/cover patterns and their relationship with land surface temperature in Nanjing, China. *Remote Sensing* **12(3)**:440 DOI 10.3390/rs12030440.

Wang M, Meng H, Bai Y, Su JH, Sha CY, Zhang M. 2013. Relationships between landscapes spatial pattern and land surface temperature in Shanghai. *Ecology and Environmental Sciences* **22(2)**:343–350 DOI 10.16258/j.cnki.1674-5906.2013.02.028.

Wang W, Shen SH, Zhao XY, Yang SB. 2011. Comparative analysis on quantitative relationships between NDVI, RSR and land surface temperature. *Resources and Environment in the Yangtze Basin* **20(4)**:439–444.

Wu ZG, Jiang T, Fan YL, Chen LJ. 2016. Land surface temperature retrieval and result analysis based on Landsat 8 data in Wuhan City. *Chinese Journal of Engineering Geophysics* **13(1)**:135–142 DOI 10.3969/j.issn.1672-7940.2016.01.023.

Wu JW, Xu JH, Tan WQ. 2007. Study on the relationship of urban heat island and vegetation abundance in Shanghai City. *Remote Sensing Technology and Application* **22(1)**:26–30 DOI 10.11873/j.issn.1004-0323.2007.1.26.

Xiao W, Hu ZQ, Fu YH. 2014. Zoning of land reclamation in coal mining area and new progresses for the past 10 years. *International Journal of Coal Science & Technology* **1(2)**:177–183 DOI 10.1007/s40789-014-0024-3.

Xie MM, Wang YL, Fu MC. 2011. An overview and perspective about causative factors of surface urban heat island effects. *Progress in Geography* **30(1)**:35–41 DOI 10.11820/dlkxjz.2011.01.004.

Xu HQ, He H, Huang SL. 2013. Analysis of fractional vegetation cover change and its impact on thermal environment in the Hetian basinal area of County Changting, Fujian Province, China. *Acta Ecologica Sinica* **33(10)**:2954–2963 DOI 10.5846/stxb201205150720.

Xu S, Li FX, Zhang LB, Zhou L. 2015. Spatiotemporal changes of thermal environment landscape pattern in Changsha. *Acta Ecologica Sinica* **35(11)**:3743–3754 DOI 10.5846/stxb201310142477.

Yang JH. 2013. Evaluation research on land sustainable use of Jixi City with Coal Resource-exhausted. M. Thesis, Northeast Agricultural University.

Ye CH, Liu YH, Liu WD, Liu C, Quan WJ. 2011. Research on urban surface heat environment monitoring indexes and its application. *Meteorological Science and Technology* **39(1)**:95–101 DOI 10.19517/j.1671-6345.2011.01.019.

You X, Yan LM. 2009. Retrieving land surface temperature from the ETM+ image radioactive transfer equation. *Sci-Tech Information Development & Economy* **19(27)**:134–136+138.

Yu XX. 2006. *Landscape ecology*. Beijing: Higher Education Press.

Yue TC, Nie S, Pan H, Li LC. 2019. Land surface temperature retrieval and urban heat island effect based on Landsat 8 image in Fuzhou City. *Journal of Northwest Forestry University* **34(5)**:154–160 DOI 10.3969/j.issn.1001-7461.2019.05.24.

Yue WZ, Xu JH, Xu LH. 2006. An analysis on eco-environmental effect of urban land use based on remote sensing images: a case study of urban thermal environment and NDVI. *Acta Ecologica Sinica* **26(5)**:1450–1460.

Zhang H, Qi ZF, Ye XY, Cai YB, Ma WC, Chen MN. 2013b. Analysis of land use/land cover change, population shift, and their effects on spatiotemporal patterns of urban heat islands in metropolitan Shanghai, China. *Applied Geography* **44**:121–133 DOI 10.1016/i.apqeoq.2013.07.021.

Zhang F, Tashpolat T, Ding JL, Mamat S, Nigala T, Gui DW, Wang JS. 2013a. The heat environment of land surface of typical oasis in upper reaches of Tarim river with remote sensing images. *Journal of Arid Land Resources and Environment* **27(4)**:111–116 DOI 10.13448/j.cnki.jalre.2013.04.014.

Zhang B, Zheng LF, Tong QX, Wang JF, Shu R, Xue YQ. 2000. Study on the retrieval of emissivity spectra from airborne thermal infrared data. *Journal of Infrared and Millimeter Waves* **19(5)**:361–365 DOI 10.3321/j.issn:1001-9014.2000.05.009.

Zhou JH, Wang LJ. 2014. Comprehensive study on ecological restoration and land exploitation of mining subsidence in suburbs of Chinese mining cities. *International Journal of Coal Science & Technology* **1(2)**:248–252 DOI 10.1007/s40789-014-0035-0.

Zhou QX, Zhang QR. 2005. Environmental problems and ecological countermeasures of coal-mining areas in the old industrial base, Northeastern China. *Chinese Journal of Ecology* **24(3)**:287–290 DOI 10.13292/j.1000-4890.2005.0254.

Zhu ZR, Cheng PG, Gui X, Teng Y, Tong CZ. 2016. Overview of surface temperature inversion algorithm. *Geomatics & Spatial Information Technology* **39(5)**:70–75 DOI 10.3969/j.issn.1672-5867.2016.05.020.